Computational modeling of intraocular drug delivery supplied by porous implants

Seyedalireza Abootorabi, Abhimanyu Tripathi, Huidan Whitney Yu & Lilian P. Dávila

Drug Delivery and Translational Research
An Official Journal of the Controlled Release Society

ISSN 2190-393X

Drug Deliv. and Transl. Res.
DOI 10.1007/s13346-020-00878-2

Springer

Drug Delivery and Translational Research
https://doi.org/10.1007/s13346-020-00878-2

ORIGINAL ARTICLE

Computational modeling of intraocular drug delivery supplied by porous implants

Seyedalireza Abootorabi[1] · Abhimanyu Tripathi[2] · Huidan Whitney Yu[1] · Lilian P. Dávila[2]

Accepted: 16 November 2020

Abstract

New and efficient drug delivery to the posterior part of the eye is a growing health necessity worldwide. Current treatment of eye diseases, such as age-related macular degeneration (AMD), relies on repeated intravitreal injections of drug-containing solutions. Such a drug delivery has major drawbacks including short drug life, significant medical service, and high medical cost. In this study, we explored a new approach to controlled drug delivery by introducing unique porous implants. Our computational modeling contained key physiological and anatomical traits. Incompressible flow in a porous media field, including the sclera, choroid, and retina layers, is governed by Darcy law and the time evolution of the drug concentration was solved via three convection–diffusion equations in the three layers, respectively. The computational model was validated by established results from independent studies and experimental data. Simulations of the IgG1 Fab drug delivery to the posterior eye were performed to evaluate the effectiveness of the porous implants for controlled delivery. Overall, our results indicate that drug therapeutic levels in the posterior eye sustain for eight weeks similarly to those using intravitreal injection. We first evaluated the effects of the porous implants on the drug delivery in the posterior layers. Subsequent simulations were carried out with varying porosity values in a porous episcleral implant. We found that the time evolution of drug concentration is distinctively correlated to drug source location and pore size. A correlation between porosity and fluid properties for selected porous implants was revealed for the first time in this study.

Keywords Drug delivery · Posterior eye · Computational modeling · Age-related macular degeneration · Transcleral delivery

Introduction

Age-related macular degeneration (AMD) is a degenerative disease of the retina layer where uncontrolled growth of cells in the blood vessels causes protein and blood leakage and scars the macula (a part of the retina layer inside the eyeball). It is a condition that often results in blurred or no vision in the central visual field. Such a vision loss is permanent, affecting people with the ability to recognize faces, drive, or perform daily activities. AMD is the leading cause of severe vision loss in people over age 60 years old [1]. According to the National Eye Institute, as the older population in the USA grows larger, more people are developing eye diseases. In fact, from 2000 to 2010, the number of elderly people with AMD grew 18%, from 1.75 million to 2.07 million [1]. It is known that vascular endothelial growth factor (VEGF), a signal protein produced by cells that stimulate the formation of blood vessels, is responsible for this eye disease condition. Anti-VEGF drugs, such as Ranibizumab, Macugen, and IgG1 Fab fragment, are frequently used to treat AMD.

An injection is a common way to deliver drugs for the treatment of AMD. However, this adds potential risks such as endophthalmitis, hemorrhage, and retinal detachment [2], among others. The oral consumption of drugs is an alternative but ineffective method to deliver the drug via blood

Seyedalireza Abootorabi is now at the Mechanical Engineering Department, University of Texas at Dallas.

✉ Lilian P. Dávila
ldavila@ucmerced.edu

[1] Department of Mechanical and Energy Engineering, Purdue School of Engineering and Technology, Indiana University-Purdue University, 723 West Michigan Street, Indianapolis, IN 46202, USA

[2] Department of Materials Science and Engineering, School of Engineering, University of California Merced, 5200 N. Lake Road, Merced, CA 95343, USA

Published online: 11 January 2021

flow. Since the blood supply into the human eye is small, a large amount of drug consumption is needed, which may put other non-diseased tissues in danger. Sclera permeability is a less risky, less invasive, and more sustainable drug transport method of drug delivery for AMD, enabling transscleral drug delivery [3, 4]. In this type of drug delivery, an implant that contains a drug is implanted on the posterior eye (AMD normally affects the posterior eye) and the drug diffuses into the eye slowly [5], providing a sustainable drug transport source.

It is essential to predict drug transport in the different layers of the posterior eye to design an effective delivery system. Drugs available for AMD have a narrow therapeutic concentration window (i.e., a limited range of drug dosages which can treat the disease effectively without having toxic effects). Medication with such a restricted therapeutic window must, therefore, be administered with care and control. High drug concentrations can be harmful to the eye, while low drug supply results in the ineffective treatment of AMD [6]. Therefore, it is crucially important to determine the time evolution of drug concentration in each layer in the posterior eye. There are experimental techniques available to measure drug concentration in the eye, such as absorption spectroscopy [7] and direct sampling [8]. Some studies have emphasized the benefits and challenges of such experiments. Miller et al. [7] have reported minimally invasive and direct measurements of drug concentration in the eye via absorption spectroscopy, whereas Conrad et al. [8] have described that direct sampling is possible but difficult for the patient.

Numerical simulation of drug delivery in the eye is a new and non-invasive method to measure the time evolution of drug concentration. This technique offers several advantages, including the ability to (i) study a system or phenomenon at different length and time scales; (ii) obtain reliable results, once well validated by available analytical and/or experimental data; (iii) perform analysis of varied conditions; (iv) evaluate critical situations that can be investigated without risk; and (v) carry out cost-effective studies that can speed up so that system or phenomenon can be evaluated over a long time. Simulations are usually much faster than experiments. In the present study, we simulate 8-week drug delivery in less than 30 min with standard CPUs of personal computers. Some of the disadvantages of simulations of drug delivery in the eye include (i) an understanding of the controlled drug delivery phenomena is needed as well as the associated limitations and approximations of the model to discern the solutions from potential artifacts, and (ii) limited experimental data [9, 10] is available regarding posterior eye layers. Several simulation studies have been reported to date investigating the drug delivery in the eye computationally by Kavousanakis et al. [11] and Balachandran and Barocas [12], in which drug delivery from a standard implant in the posterior eye is simulated using the finite element method (FEM) and drug concentration evolution is calculated for different eye layers. Other studies [13–15] have focused on computational modeling to simulate the intravitreous drug injection in the human eye.

The thermally responsive hydrogel (N-isopropyl acrylamide) NIPAM has been used to evaluate ocular drug delivery computationally [11, 16] by placing it on the sclera close to the optical nerve. Previous simulations of drug delivery from an episcleral NIPAM-gel implant by Ninawe et al. [16] predicted sustained delivery times of 8 weeks with both 1.0 and 0.5 mg monthly doses using a compartmental model. Later, simulations by Kavaousanakis et al. [11], using a computational model of IgG1 Fab delivery from an episcleral NIPAM-gel implant, released the drug at the same rate and monthly doses as in Ninawe et al. [16] in a new model of the human eye to determine the time needed for sustained delivery. Results from the latter study [11] show that the average drug concentration is at therapeutic levels within all three layers in the posterior eye during the first 8 weeks after drug administration, similarly to those with intravitreal injection and related [15, 17, 18]. Kavaousanakis and co-workers [11] concluded that delivery of the IgG1 Fab drug from an episcleral NIPAM-gel implant seems to be an effective alternative to more invasive means of delivery to the posterior eye by injection. Thus, we used these results in our validation phase in this work. Since we need to keep the drug concentration in the desired therapeutic range, it is imperative to use the proper amount of drug concentration. It is noteworthy that we excluded the vitreous humor and confined our simulations to the eye posterior layers (sclera, choroid, and retina) from a porous implant.

In this study, we present a new computational model of a drug storage (implant) in which a porous separator or divider is introduced (inside the implant itself) and simulate the drug delivery to the posterior eye. The research objective is to achieve an appropriate time evolution of the drug concentration, avoiding the overshooting of drug concentration at initial times and increasing the later concentration. This can be done by changing the implant internal structure and including pores. We keep the drug concentration in the desired therapeutic range. The computational model includes the posterior eye layers (sclera, choroid, and retina) and drug storage. We first validate our computational model by repeating the results in Kavousanakis et al. [11]. Then, we systematically investigate how the porous structure in the implant affects drug delivery. The remainder of this paper is organized as follows: The "Computational modeling, governing equations, and validation" section describes the computational model, governing equations, and validation. The simulation results and discussion are presented in the "Numerical results and discussion" section, followed by conclusions in the "Conclusions" section.

Computational modeling, governing equations and validation

Human eye representative and computational modeling

To study the effects of implant structure on the drug delivery to the posterior eye, we created a model representative of the human eye together with an implant attached to the sclera layer on the back of the eye. Figure 1(a) illustrates a cross-sectional view of the human eye. The vitreous humor is a gel-like porous medium, which comprises most of the interior of the eye. It is enclosed by the retina layer on the posterior eye and by the lens and hyaloid membrane on the front side of the eye.

The front side of the eye (i.e., lens and pupil) were not be taken into account in this study because they are almost impermeable to drugs as there is constant flow drainage between the iris and lens, which washes any drug away. Since the transport of macromolecules such as IgG1 Fab is not significant in the front of the eye (cannot penetrate the hyaloid membrane) and the drug for the AMD targets the three posterior layers, the vitreous humor was not included in this study either.

Figure 1(b) shows the 2D axisymmetric model consisting of posterior layers (retina, choroid, and sclera) and a drug storage implant with a porous structure. This 2D model can be extended to a 3D domain to form a spherical shell through a rotation along the pupillary axis, covering the three posterior layers, which will be closer to the real eye model. We used COMSOL Multiphysics version 5.4 (COMSOL, Inc., Burlington, MA) to simulate the delivery of IgG1 Fab drug from the porous implant to the posterior layers. The main physical property values and dimensions were based on experimental data [11, 12], as summarized in Table 1. Boundary conditions were introduced as follows. The pressure at the outer surface of the sclera layer, P_s (= 1300 Pa) known as previously reported [19, 20]. The pressure at the hyaloid membrane and the interface of the retina and vitreous humor is equal to the intraocular pressure, i.e., P_h(= 2000Pa) [11].

The hyaloid membrane is a layer permeable to small drugs such as fluorescein but impermeable to heavier drug molecules such as IgG1 Fab. There is no concentration gradient at the sclera's and retina's external walls, and the implant's walls, i.e., $\hat{n} \bullet D\nabla c|_{wall} = 0$, in which $\hat{n}$ is the normal vector to the surface, D is the diffusion coefficient, and c is the drug concentration. The initial velocity is considered zero for the entire domain as well as zero concentration of the drug. The specific location of the drug supply will be identified later ("Validation: drug delivery via hydrogel implant"). The numbers of mesh in the radial direction are 3 in the retina and choroid layers and 4 in the sclera layer, respectively. The number of mesh in the tangential direction is 1400. The distribution of the mesh in each direction is uniform. The convergence check is done for the considered mesh size.

The parameters used in the simulations for the transport of the IgG1 Fab fragment are summarized in Table 1.

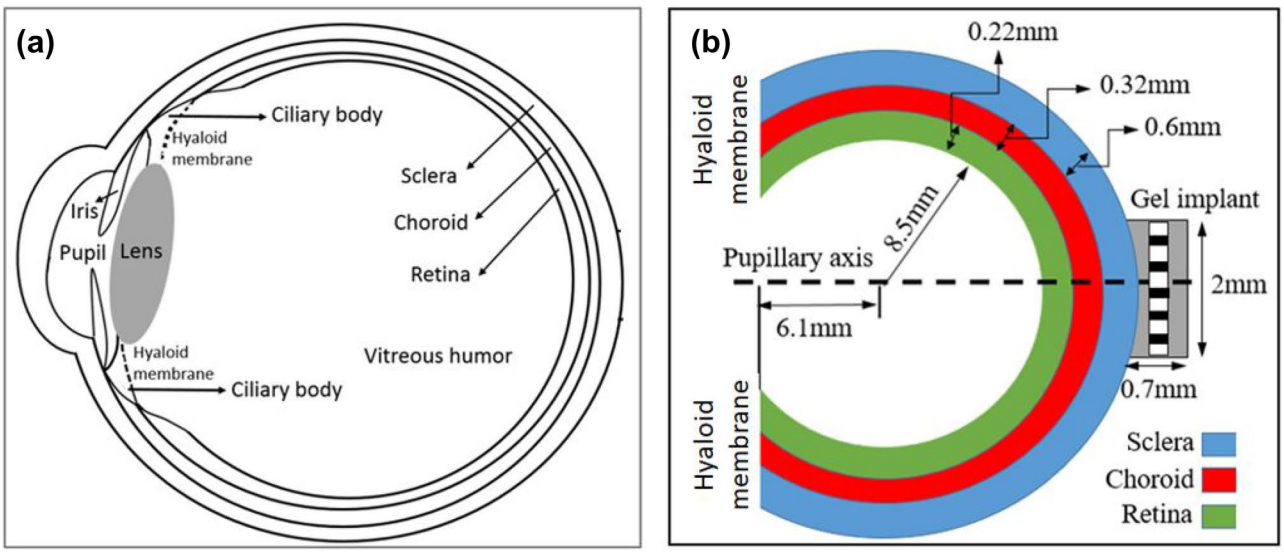

Fig. 1 Schematics of a cross section of the human eye showing an episcleral implant and key features. (a) An anatomical view of the posterior segment consisting of three distinct layers (sclera, choroid, and retina). (b) Computational geometry involving the posterior layers (retina, choroid, and sclera) and a drug storage implant with a porous separator (white and black squares mean solid pieces and pores, respectively). Dimensions are to scale. Relevant dimensions and properties are listed in Table 1

Table 1 Physical property values for the posterior eye layers and implant in this study

Parameter	Value	Source
Sclera (outer layer)		
Hydraulic conductivity $(K/\mu)_s$	1.5×10^{-11} cm^2/Pa s	Fatt and Hedbys [21]; Balachandran and Barocas [12]
Thickness (d_s)	0.6 mm	Missel [15]
Diffusivity (D_s)	4.596×10^{-7} cm^2/s	Ninawe et al. [16]
Choroid (middle layer)		
Hydraulic conductivity $(K/\mu)_c$	1.5×10^{-11} cm^2/Pa s	Fatt and Hedbys [21]; Balachandran and Barocas [12]
Thickness (d_c)	0.32 mm	Missel [15]
Diffusivity (D_c)	3.616×10^{-8} cm^2/s	Ninawe et al. [16]
Drug elimination rate constant (k_{ec})	0.2398 day^{-1}	Ambati et al. [4]
Retina (inner layer)		
Hydraulic conductivity $(K/\mu)_r$	2.36×10^{-11} cm^2/Pa s	Tsuboi [17]
Thickness (d_r)	0.22 mm	Missel [15]
Diffusivity (D_r)	2.442×10^{-7} cm^2/s	Ninawe et al. [16]
Drug elimination rate constant (k_{er})	0.2063 day^{-1}	Ambati et al. [4]
Implant with porous separator		
Diffusivity (D_i)	6.0×10^{-6} cm^2/s	Hettiaratchi et al. [18]
Rectangular shaped, radius	0.10 cm	Kavousanakis et al. [11]; Ninawe et al. [16]
Rectangular shaped, width	0.70 mm	n/a
Separator, width	0.045 mm	n/a
Separator, pore size (d)	0.008–2.0 mm	n/a

Mathematical model and governing equations

The flow domain, including the sclera, choroid, and retina layers in Fig. 1(b), is treated as a porous medium. The eye drug is stored in the implant and delivered to the posterior layers. As the flow in the sclera, choroid, and retina layers is weak, we used the Darcy (creeping) flow equation. The creeping flow equation is coupled with the diffusion equations to reflect the convective drug transfer. We, therefore, focused on the diffusion and convection of IgG1 Fab drug doses to the posterior layers.

Diffusion flow model for the IgG1 Fab drug

The porous media flow in the posterior layers is assumed incompressible and governed by the following Darcy flow equation:

$$v = -\frac{K}{\mu}\nabla P \tag{1}$$

where $\boldsymbol{v}$, K, μ, and P are the flow velocity, the permeability of the medium, the viscosity, and the pressure of the fluid, respectively.

Diffusion-convection equations for the sclera, choroid, and retina layers

Drug diffusion through the layers of the posterior eye is modeled by Fick's first law. As seen in Fig. 1(b), the drug solution (IgG1 Fab) is released in the gel implant and delivered to the posterior eye. Molecular diffusion is deemed the main driving mechanism for drug transfer through the layers of the posterior eye. For calculating the transport of the drug through the layers of the posterior eye, we introduce the diffusion-convention equation in each layer of the posterior eye as follows:

Sclera (outer) layer:

$$\frac{\partial c_s}{\partial t} - D_s\nabla^2 c + \boldsymbol{v} \bullet \nabla \mathrm{c} = 0 \tag{2}$$

Choroid (middle) layer:

$$\frac{\partial c_c}{\partial t} - D_c\nabla^2 c + k_{ec}c + \boldsymbol{v} \bullet \nabla \mathrm{c} = 0 \tag{3}$$

Retina (inner) layer:

$$\frac{\partial c_r}{\partial t} - D_r\nabla^2 c + k_{er}c + \boldsymbol{v} \bullet \nabla \mathrm{c} = 0 \tag{4}$$

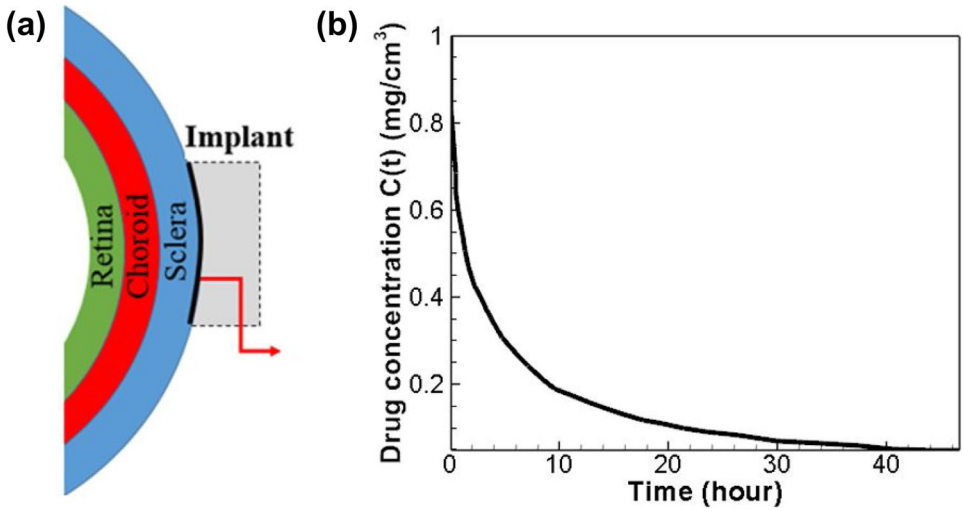

Fig. 2 The setup of IgG1 Fab drug in a hydrogel implant. Illustrations show (a) the drug source is placed on the hydrogel implant-sclera interface (black line) and (b) the exponential decay of the drug concentration at the implant when $C(t=0) = C_o = 1$ mg/cm^3 [16]

In Eqs. (2)–(4), D_s, D_c, and D_r are the drug diffusivities in the sclera, choroid, and retina layers, respectively, and k_{ec} and k_{er} are rate constants of drug elimination due to the absorption to the veins in the choroid and retina, respectively. There is no drug elimination in the sclera, and thus, there is no rate constant of drug elimination in Eq. (2).

Validation: drug delivery via hydrogel implant

IgG1 Fab is a macromolecular anti-VEGF drug routinely used to treat AMD. Experimental data on IgG1 Fab drug concentration in the layers of the posterior eye for intravitreal (IVT) injection or delivery from a local implant is not currently available. Clinical studies have shown that the therapeutic effects of drug doses of 0.5 and 1 mg/cm^3, regularly delivered by IVT injection, extend for 2 months [20]. In this section, we validate our simulation with independently reported data [11] for the delivery of IgG1 Fab to the layers of the posterior eye using a hydrogel implant (Fig. 2(a)). Then, we simulate the episcleral delivery of IgG1 Fab drug to the layers of the posterior eye via a new type of porous implant (Fig. 2(b)). The parameters used in the simulations for the transport of the IgG1 Fab fragment are shown in Table 1.

To validate our computational modeling with previous experimental and computational studies [11, 16], we placed the IgG1 Fab drug source on the left inner wall of a hydrogel implant, as seen in Fig. 2(a), to study drug delivery to the posterior layers. On the implant's inner wall, the drug concentration is set to decay exponentially for 2 days of release, as seen in Fig. 2(b).

We focus on the drug delivery across the posterior layers in terms of the time evolution of the drug concentration and drug delivery velocity across the layers. Figure 3(a) shows

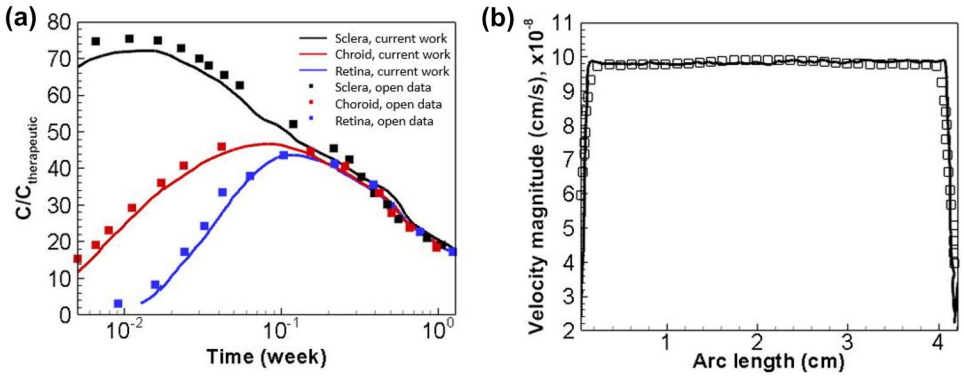

Fig. 3 Validation results regarding drug delivery to the posterior layers. Calculations show (a) time evolution of the average IgG1 Fab drug concentration in the sclera (black), choroid (red), and retina (blue) layers, respectively. Solid lines are the results of the current simulations and solid squares are data from a previous study by Kavousanakis et al. [11]. The velocity profile (b) along the choroid-sclera shows agreement with prior findings [11]. The solid line is from the current simulation and the open squares are from reported open data reported by Kavousanakis and co-workers [11]

the time evolution of the average IgG1 Fab drug concentration in the sclera (black), choroid (red), and retina (blue) layers within 2 months after administration begins, for a monthly dose, $C_o = 1$ mg/cm^3. Drug concentrations have been normalized with the therapeutic concentration value of $C_{therapeutic} = 150$ mg/cm^3 [11]. This therapeutic concentration is the minimum required concentration of the drug that must exist to have an effective treatment. The corresponding solid symbols are computational results from a previous study [11].

Because of the very high amount of the initial drug concentration at the implant, there is a high value of drug concentration at the beginning in the three different layers (Fig. 3(a)). By the time the drug source weakens and the drug absorption overpowers the drug transfer from the implant, the concentration shows a decline. The velocity profile along the choroid-sclera interface is shown in Fig. 3(b). The rapid change of the velocity at the beginning and the end of the graph can be attributed to the fact that there is a sharp pressure gradient between the outer surface of the sclera and the hyaloid membrane and the measurement starts to close the intersection of the sclera and the hyaloid membrane. The pressure gradient is uniform through the rest of our arc because the distance between the retina's outer surface and sclera's outer surface remains the same. Also, Fig. 4 shows the logarithmic distribution of the normalized drug concentration on the entire domain at 8 hours (top row) and 8 weeks (bottom row). Our simulation results (right column) are comparable to those from open data reported by Kavousanakis et al. [11]. Overall, our simulation results have well reproduced the spatial–temporal drug delivery of IgG1 Fab placed on the hydrogel implant-sclera interface (black line) in Fig. 2(a) to the posterior layers of Fig. 1(b).

Furthermore, the time evolution of the normalized drug concentration in 8 weeks at three representative locations in the retina layer is shown in Fig. 5(a)-(c), respectively, with the locations indicated in Fig. 5(d). The three locations at 1, 2, and 3 reach the peak concentration after 0.063, 1.13, and 1.97 weeks, with normalized peak concentration of 1232.6, 7.3, and 1.5, respectively.

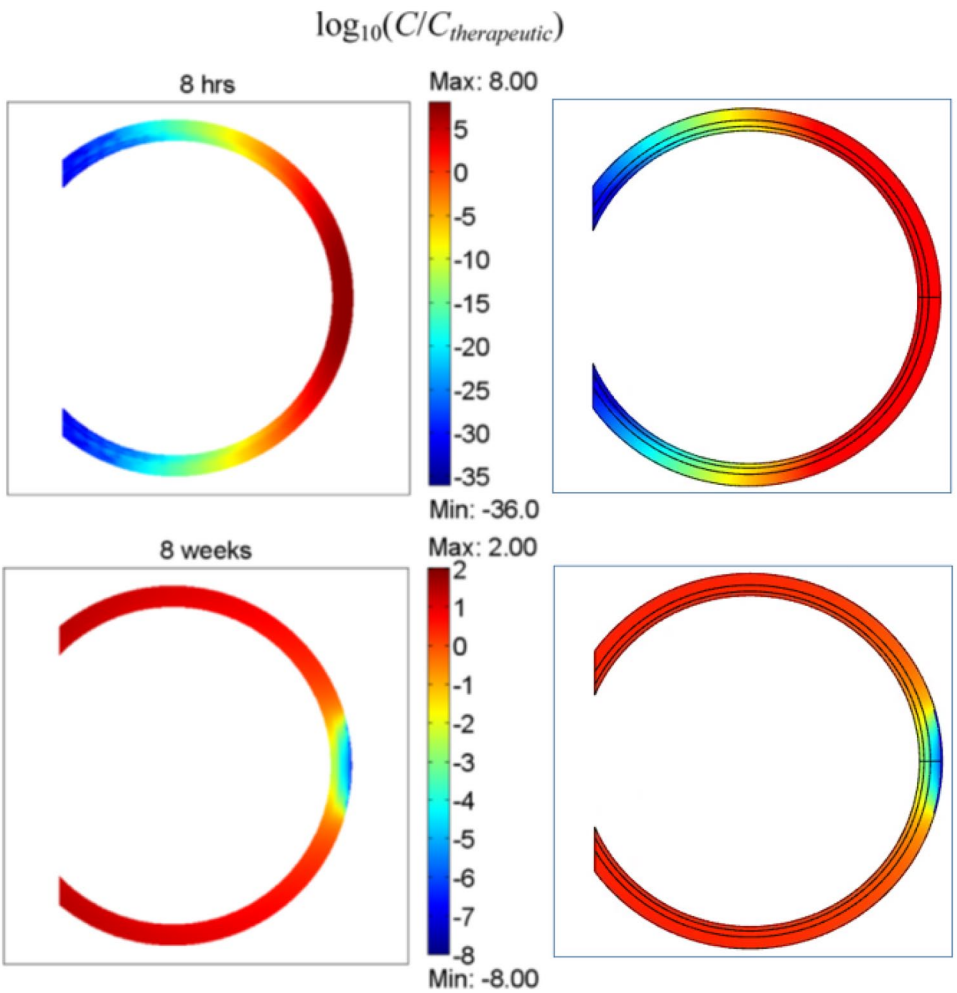

Fig. 4 Spatial concentration distribution of the drug, $\log_{10}(C/C_{therapeutic})$, in the xz-plane through the sclera, choroid, and retina layers, when the initial drug concentration at the implant-sclera interface is $C_o = 1$ mg/cm^3: 8 hours (top row) and 8 weeks (bottom row), respectively. Our simulation results (right column) are consistent to the open data from a previous study (left column) [11]

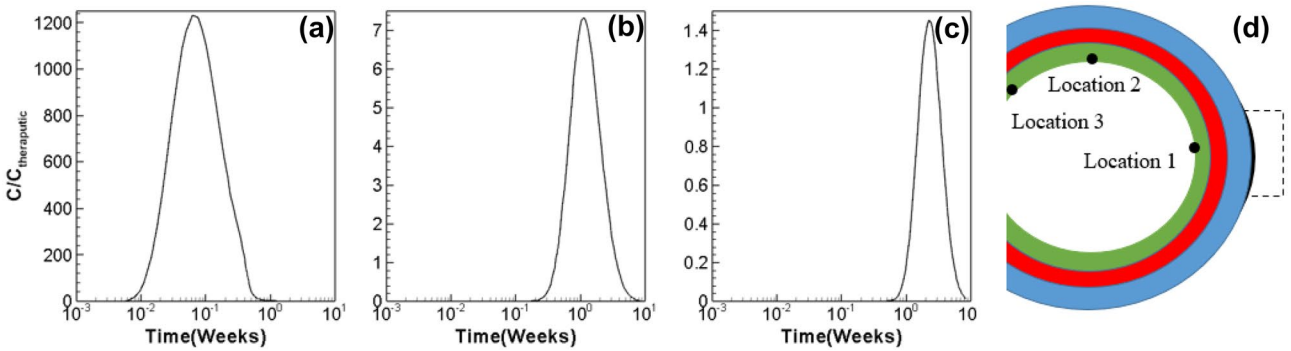

Fig. 5 Time evolution of normalized drug concentration in 8 weeks at three specific locations in the retina layer, namely, (a) location 1, (b) location 2, and (c) location 3, as indicated in (d)

Numerical results and discussion

In this section, we investigated the effects of implant setup and implant structure on drug delivery. We studied the role of drug source location on the concentration levels calculated in the posterior eye layers. Then, we conducted simulations of the delivery of IgG1 Fab to the posterior layers using a porous implant. In this case, we analyzed the effect of pore size on drug concentration evolution and compared results against the former standard hydrogel implant. All these results and analysis are described next.

Role of drug source location

The previous study placed the drug on the left inner wall of the implant, Fig. 2(a), which has eliminated the functionality of the implant. Here, we explore the effect of drug source location in the implant on the drug delivery in the posterior eye layers. Figure 6 shows the time evolution of the IgG1 Fab drug concentration in the three posterior layers using two different drug source locations in the implant: (a) left wall and (b) right wall. It is evident from these results that the location of the drug source (i.e., concentration boundary condition) is important to consider in the evolution of the mean drug concentration. Placing the drug source in the *sclera-implant* interface (case (a)) was found to be more accurate when comparing data against prior simulations [11] than the alternative (case (b)). This despite the fact our implant dimensions are smaller than those reported before by Kavousanakis et al. [11], yet the concentration levels and trends are similar as demonstrated in Fig. 3(a). It is reasonable to expect drug concentration levels in the eye layers to be higher in case (a) than in case (b)—where drug transport will require more time to reach all three layers, and thus concentration levels will decrease. Note also that case (a) has an enlarged *sclera-implant* interface (i.e., length of black line) compared to case (b) and hence the higher values.

Furthermore, as seen in Fig. 6, the drug concentration curves show higher peaks for case (a) than case (b) in all three layers. This can be attributed to the fact that drug spreads into the eye faster than it gets eliminated, and concentration peaks are higher since the drug source is closer to the eye layers or in "direct contact with the sclera." However, the drug source will change location (case (b)) for an implant containing a porous separator as in Fig. 7(a), which will essentially create a diffusion barrier to drug transport and further slowdown drug diffusion (Diffusion through porous implants: pore size effect").

Diffusion through porous implants: pore size effect

The objective of the current research is to explore a new implant with a porous media structure that can efficiently

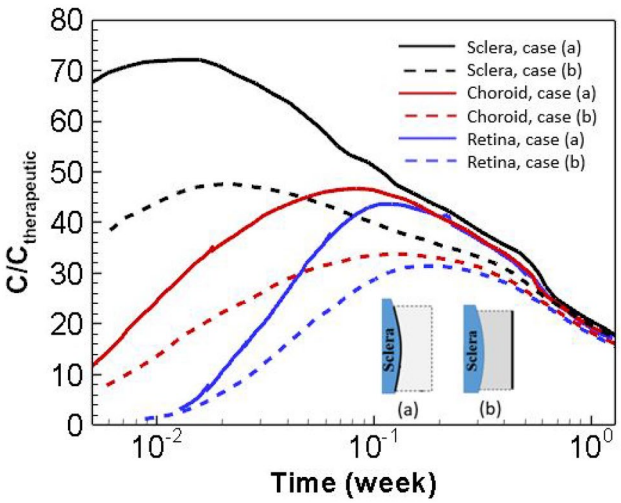

Fig. 6 Time evolution of the average IgG1 Fab drug concentration in the sclera (black), choroid (red), and retina (blue) layers, during the first 2 months after administration begins. The drug sources are placed on the (a) left wall (case a) and (b) right wall (case b) of the implant

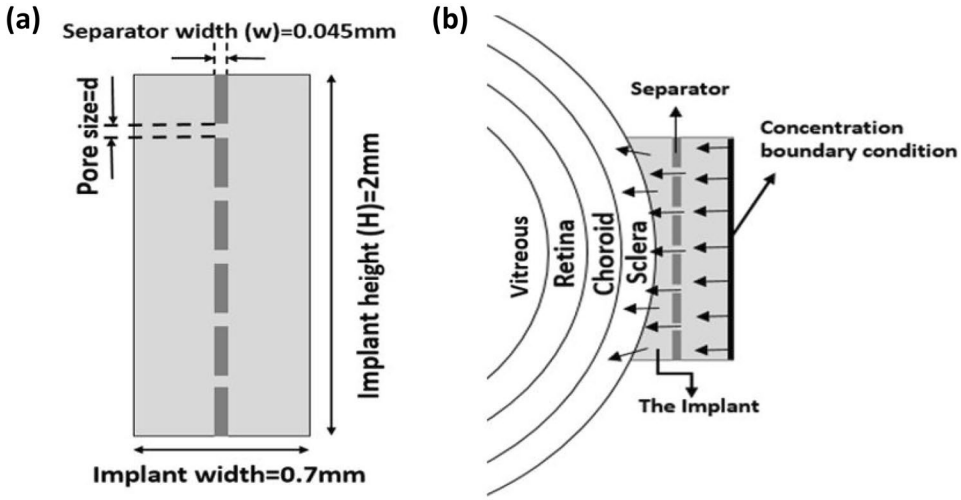

Fig. 7 Illustration of the porous implant structure comprising of a single separator with adjustable pore size. The diagrams show (a) key dimensions of the implant and (b) implant position next to the sclera, arrows indicating drug flow towards posterior layers. In this study, the IgG1 Fab drug source location is placed on the right inner wall of the implant

control drug delivery in the posterior eye. In this study, we introduce a single separator in the implant to mimic the porosity of a porous media structure, as seen in Fig. 7(a), and study the effects of the separator traits (i.e., pore size) on the drug delivery. The physical properties of this implant are the same as the physical properties of the sclera (i.e., diffusion coefficient and permeability). As shown in Fig. 7(b), the drug is placed on the right inner wall of the implant with the same concentration decay as in Fig. 2(b). The pore arrangement is adjustable therefore the drug release to the posterior layers can be precisely controlled through the porosity of the porous media structure.

The concept of introducing porous barriers (separators) within an implant is used in this study to examine the effect of porosity on drug release. Since the drug source (concentration boundary condition) is placed on the right side of the porous implant as in Fig. 7(b), this allows the evaluation of pore sizes inside the implant for sustained drug delivery in a systematic manner.

We have used different pore diameters in a separator inside a hydrogel implant (Fig. 7(a)) to examine their effect on drug concentration to the posterior eye layers. Clinical studies with IgG1 Fab, delivered by IVT injection, have reported that the time during which the drug concentration in the choroid and retina layers is at a therapeutic level is about 8 weeks [20]. Figure 8 summarizes the evolution of drug concentration in each of the eye layers (sclera, choroid, and retina) as a function of pore diameter during this period of interest. Drug concentrations have been normalized with the therapeutic concentration ($C_{therapeutic} = 150\ \mu g/l = 150\ mg/cm^3$), which completely inhibits neovascularization. As Fig. 8 shows, the average drug concentrations in the sclera (a) remains higher at all times compared to those in the choroid (b) and the retina (c). This can be attributed to the fact that the released drug in the latter (b) and (c) has to pass through the implant and larger sclera, diffusing at a lower speed into the eye due to differences in diffusivity values and drug elimination rates. Note also that the average drug concentration is at therapeutic levels within all three layers throughout the first 2 months after dose administration began.

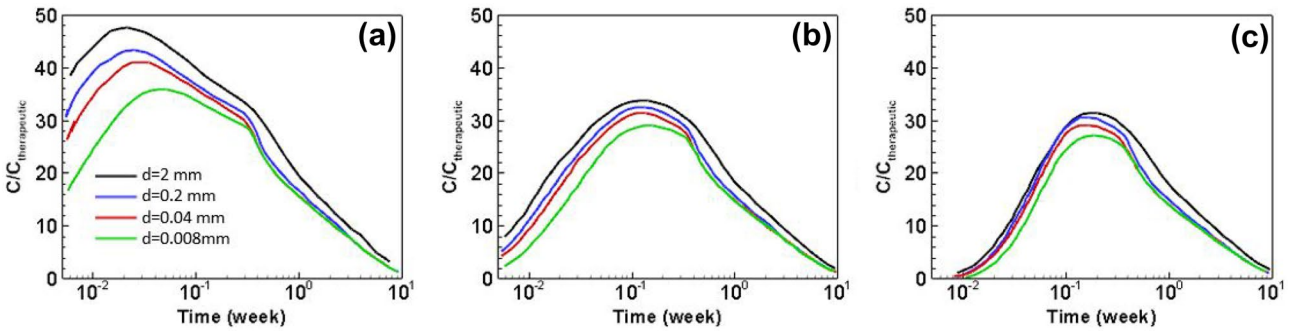

Fig. 8 Average drug concentration in the (a) sclera, (b) choroid, and (c) retina using a porous implant, as a function of pore sizes as shown in Fig. 7(a), during the first 2 months after administration begins and where $c_o = 1\ mg/cm^3$. Legend denotes pore size vary in diameter *d* in case: 2, 0.2, 0.04, and 0.008 mm

Results in Fig. 8 indicate that the average drug concentration levels in all three layers are lower for the porous implant than those for the standard hydrogel implant in Fig. 3(a). This is expected as the drug source is located as in Fig. 7(b) and Fig. 6(b). The porous separator is essentially a barrier to drug diffusion, and thus, drug concentration levels are expected to diminish. The trends in Fig. 8(a-c) show that all drug concentration curves increase at the beginning until they reach a maximum value (peak) before decreasing rapidly for all pore sizes. The differences in drug concentrations in Fig. 8(a-c) can be explained as follows. It will likely take more time for the drug to diffuse through the porous implant (than the standard implant) and reach all three layers, and given the different diffusivities per layer, the average drug concentrations would be lower in each subsequent inner layer (i.e., sclera > choroid > retina with the lowest drug concentrations) as seen in Fig. 8(a-c).

More significantly, results in Fig. 8 show that as pore size decreases in the porous implant so does the average drug concentration in all three layers. Figure 8 suggests a correlation between pore size and drug concentration (i.e., the smaller the pore diameter is the lower the average drug concentration is in each layer and vice versa). The average drug concentration profiles reveal distinct peaks in the layers, in particular in the sclera (Fig. 8(a)). It is noteworthy that as pore diameter shrinks, the drug diffuses through the porous implant into the sclera faster (Fig. 7(b)) than veins can eliminate the drug, and thus, drug concentration increases in the sclera.

Conclusions

In summary, the overall findings from this study indicate that drug source location and morphological features such as pores within the porous implants have measurable effects on the fluidic behavior in the posterior eye layers (sclera, choroid, and retina). Specifically, the role of a porous separator with varied small pores contributes distinctively to the overall fluidic response of the implant. While the very small pores lead to dissimilar behaviors of average drug concentrations in each posterior eye layer, as the pore diameter shrinks this behavior reduces the average drug concentration of the sclera more significantly. This suggests the pores in the implant could be tailored further to control other variables such as drug release rates, other drugs, patient needs, etc. To validate this hypothesis, further studies are necessary to determine whether it is valid to assume there are implant morphologies that can lead to optimum drug delivery rates. Future directions regarding simulations will include investigating the effect of separator thickness, drug type on drug delivery, and role of the diffusion coefficient as it is an important parameter in drug transport and its effects need to be investigated further for different routes of delivery and optimum drug delivery devices for controlled release applications [22–24].

Acknowledgments This work was performed under the auspices of an IU-STEM faculty collaborative award at the University of California, Merced and Indiana University-Purdue University, which provided seed funds and support for co-authors (AT, SA) at the University of California, Merced, and Indiana University-Purdue University respectively. Dedicated to the memory of Drs. Luis and Glicerio Dávila Negrón, a legacy of love for medicine and people (father and uncle of co-author LD).

Author contributions All authors participated in the writing of the manuscript. Both Dr. Lilian Davila and Dr. Whitney Yu planned and supervised the work.

Funding This work received funds from Indiana University through a MSI Seed Funding – STEM Initiative, award number 18–0512.

Compliance with ethical standards

Conflict of interest The authors declare that they have no conflict of interest.

Consent for publication All authors consent the publication.

References

1. The National Eye Institute. Age-related macular degeneration (AMD) data and statistics. NIH Publishing. 2020. https://www.nei.nih.gov/learn-about-eye-health/resources-for-health-educators/eye-health-data-and-statistics/age-related-macular-degeneration-amd-data-and-statistics. Accessed 5 Jan 2020.
2. Geroski DH, Edelhauser HF. Drug delivery for posterior segment eye disease. Invest Ophth Vis Sci. 2000;41(5):961–4.
3. Ahmed I, Patton T. Importance of the noncorneal absorption route in topical ophthalmic drug delivery. Invest Ophth Vis Sci. 1985;26(4):584–7.
4. Ambati J, Gragoudas ES, Miller JW, You TT, Miyamoto K, Delori FC, Adamis AP. Transcleral delivery of bioactive protein to the choroid and retina. Invest Ophth Vis Sci. 2000;41(5):1186–91.
5. Myles ME, Neumann DM, Hill JM. Recent progress in ocular drug delivery for posterior segment disease: Emphasis on transcleral iontophoresis. Adv Drug Deliv Rev. 2005;57(14):2063–79.
6. Patel A, Cholkar K, Agrahari V, Mitra AK. Ocular drug delivery systems: An overview. World J Pharmacol. 2013;2(2):47–64.
7. Miller J, Wilson WS, Wilson CG, Uttamchandani D. Minimally invasive, direct, real time measurement of drug concentration in the anterior eye. Br J Ophthalmol. 2005;89(9):1147–51.
8. Conrad JM, Robinson JR. Aqueous chamber drug distribution volume measurement in rabbits. J Pharm Sci. 1977;66(2):219–24.
9. Engler CB, Sander B, Larsen M, Dalgaard P, Lund-Andersen H. Fluorescein transport across the human blood-retina barrier in the direction vitreous to blood. Quantitative assessment in vivo Acta Ophthalmol. 1994;72(6):655–62.
10. Dalgaard P, Larsen M. Fitting numerical simulations of differential equations to experimental data: A case study and some general remarks. Biometrics. 1990;46:1097–109.

11. Kavousanakis ME, Kalogeropoulos NG, Hatziavramidis DT. Computational modeling of drug delivery to the posterior eye. Chem Eng Sci. 2014;108:203–12.
12. Balachandran RK, Barocas VH. Computer modeling of drug delivery to the posterior eye: Effect of active transport and loss to choroidal blood flow. Pharm Res. 2008;25(11):2685–96.
13. Kathawate J, Acharya S. Computational modeling of intravitreal drug delivery in the vitreous chamber with different vitreous substitutes. Int J Heat Mass Transf. 2008;51(23):5598–609.
14. Jooybar E, Abdekhodaie MJ, Farhadi F, Cheng YL. Computational modeling of drug distribution in the posterior segment of the eye: Effects of device variables and positions. Math Biosci. 2014;255:11–20.
15. Missel PJ. Simulating intravitreal injections in anatomically accurate models for rabbit, monkey, and human eyes. Pharm Res. 2012;29(12):3251–72.
16. Ninawe PR, Hatziavramidis D, Parulekar SJ. Delivery of drug macromolecules from thermally responsive gel implants to the posterior eye. Chem Eng Sci. 2010;65(18):5170–7.
17. Blondeau P, Tétrault JP, Papamarkakis C. Diurnal variation of episcleral venous pressure in healthy patients: A pilot study. J Glaucoma. 2001;10(1):18–24.
18. Kourlas H, Abrams P. Ranibizumab for the treatment of neovascular age-related macular degeneration: A review. Clin Ther. 2007;29(9):1850–61.
19. Fatt I, Hedbys BO. Flow of water in the sclera. Exp Eye Res. 1970;10(2):243–9.
20. Tsuboi S. Measurement of the volume flow and hydraulic conductivity across the isolated dog retinal pigment epithelium. Invest Ophth Vis Sci. 1987;28(11):1776–82.
21. Hettiaratchi MH, Schudel A, Rouse T, Garcia AJ, Thomas SN, Guldberg RE, McDevitt TC. A rapid method for determining protein diffusion through hydrogels for regenerative medicine applications. APL Bioeng. 2018;2:0261101–02611014.
22. Christopher K, Chauhan A. Contact lens based drug delivery to the posterior segment via iontophoresis in cadaver rabbit eyes. Pharm Res. 2019;36(87):1–12.
23. Timko BP, Whitehead K, Gao W, Kohane DS, Farokhzad O, Anderson D, Langer R. Advances in drug delivery. Annu Rev Mater Res. 2011;41:1–20.
24. Fenton OS, Olafson KN, Pillai PS, Mitchell MJ, Langer R. Advances in biomaterials for drug delivery. Adv Mater. 2018;30:1705328–87.